Liquid-crystalline Blue Phase stabilization by CoPt-decorated reduced-graphene oxide nanosheets dispersed in a chiral liquid crystal

Marta Lavrič,[1, a)] George Cordoyiannis,[2, 3, 4, b)] Vasileios Tzitzios,[4, 5] Ioannis Lelidis,[3] Samo Kralj,[6] George Nounesis,[4] Slobodan Žumer,[1, 7] Matej Daniel,[2] and Zdravko Kutnjak[1, 8]

[1)]*Condensed Matter Physics Department, Jožef Stefan Institute, 1000 Ljubljana, Slovenia.*

[2)]*Faculty of Mechanical Engineering, Czech Technical University in Prague, 16600 Prague 6, Czech Republic.*

[3)]*Department of Physics, National and Kapodistrian University of Athens, 15784 Zografou, Greece.*

[4)]*Biomolecular Physics Laboratory, National Centre for Scientific Research "Demokritos", 15310 Aghia Paraskevi, Greece.*

[5)]*Institute of Nanoscience and Nanotechnology, National Centre for Scientific Research "Demokritos", 15310 Aghia Paraskevi, Greece.*

[6)]*Faculty of Natural Sciences and Mathematics, University of Maribor, 2000 Maribor, Slovenia.*

[7)]*Faculty of Mathematics and Physics, University of Ljubljana, 1000 Ljubljana, Slovenia.*

[8)]*Jožef Stefan International Postgraduate School, 1000 Ljubljana, Slovenia.*

We report on the effect of reduced-graphene oxide nanosheets decorated by CoPt nanoparticles on the Blue Phase range of a chiral liquid crystal. By means of high-resolution ac calorimetry and polarizing optical microscopy it is demonstrated that a small concentration of these nanosheets induces the stabilization of a single blue phase structure in comparison to three blue phases existing in the pure compound. The results are compared with other liquid crystal-dispersed graphene studies and, moreover, a short theoretical discussion of the stabilization effect is included.

PACS numbers: 64.70.mj, 64.70.mf, 61.30.Mp, 42.70.Df, 81.05.ue

[a)]Corresponding author: marta.lavric@ijs.si

[b)]Corresponding author: georgios.kordogiannis@fs.cvut.cz

I. INTRODUCTION

Blue phases (BPs) constitute a fascinating class of liquid-crystalline structures appearing in a short temperature range between the Isotropic (I) and the chiral Nematic (N^*) phases[1]. Although there were present among the premier observation of liquid-crystalline states of cholesteryl acetate[2], they were brought into attention of research community several decades later[3,4]. Three blue phases, namely blue phase III (BPIII), blue phase II (BPII) and blue phase I (BPI) upon decreasing temperature, were observed in several chiral compounds[5–7] and the first phase diagrams were drawn as a function of chirality strength[8]. Their thermodynamic stability was proven by Thoen[9] in terms of adiabatic scanning calorimetry measurements, clearly identifying distinct anomalies for phase transitions I-BPIII, BPIII-BPII, BPII-BPI and BPI-N^* for cholesteryl nonanoate. The critical behavior as a function of chirality was also explored[10,11] and, finally, an elaborate temperature-chirality phase diagram was experimentally derived[12], demonstrating the existence of a critical point for the I-BPIII transition at strong chiralities and a triple point where all three BPs coexist. Following meticulous theoretical work presented evidense that the I-BPIII transition belongs to the three-dimensional Ising universality class, based on mean-field as well as scaling analysis of available thermal and optical experimental data[13].

By the late 90s the thermodynamic stability of BPs was confirmed in short temperature intervals (ranging typically from 1 K to 3 K between the I and the N^* phases) for several liquid-crystalline compounds. Soon after there was born the idea of using the cubic structures of BPs with lattice periodicity in the range of visible light as tunable photonic crystals[14,15]. At the same time, an emerging need appeared to increase the temperature stability range of BPs in order to boost their potential for applications. The strategies of polymer stabilization[16,17] and chiral doping[20,21] were among the first used. Wide-range, supercooled or polymer-stabilized BPs were also reported[17,22–24]. Several studies addressed the electro-optical properties (Kerr constant, driving voltage, response time) of polymer-stablized BPs, exploring their potential towards optical displays[18,19]. In the last ten years various types of nanoparticles have been also tested experimentally as stabilizing agents for BPs. These nanoparticles have either spherical cores composed of Au, CdSe, ZnS, Ni[25–32] or anisotropic laponite, graphene/graphene oxide and MoS_2 ones[33–37]. Additional studies have focused on the thorough understanding of the BP structures in pure compounds as well as their stabilization under the presence of guest components and confinement[38–43].

Here we report on the effect of reduced-graphene oxide nanosheets decorated with CoPt

nanoparticles on the BP range of the chiral liquid crystal 4-(2-methyl butyl) phenyl 4-n-octylbiphenyl-4-carboxylate (CE8). Graphene oxide nanosheets coated with oleyl amine chains (without CoPt) of same concentration and size were dispersed in CE8 in one of our previous studies on BPs[34], promoting mostly the stabilization of BPI with respect to the pure compound. Henceforth, it will be explored how the modified surface chemistry of reduced-graphene oxide affects the blue phase stabilization. It has been reported that the dispersion of a small amount of graphene nanosheets in BPs significantly improves the driving voltage, without any noticeable degradation of other electro-optical properties[44]. Hence, the deeper understanding of the role of surface-functionalization on the trapping of nanosheets in the disclination lines of BPs is essential. Moreover, the CoPt nanoparticles add multi-functionality to the final soft nanocomposite by hybridizing the LC properties with ferromagnetism. In a recent study it is shown that such CoPt-decorated, reduced-graphene oxide nanosheets assemble between the smectic layers of CE8[45].

II. MATERIALS AND METHODS

The high-purity ferroelectric liquid-crystalline compound CE8 has been purchased from Merck and used without any further treatment. The reduced-graphene oxide nanosheets have been synthesized in NCSR "Demokritos" (Greece). The actual difference between reduced-graphene oxide (r-GO) and graphene oxide (GO) lies in the reduced presence of oxygen functional groups in the former. Pristine GO is synthesized using a modified Staudenmaier's method[46]. The synthesis of CoPt-decorated r-GO nanocomposite is carried out following a liquid phase methodology similar to the one described in Ref.[47]. Briefly, GO is dispersed in oleyl amine and sonicated by the drop-wise addition of $Co(acac)_2$ and $Pt(acac)_2$ solution in octadecane/oleyl amine. Note that the r-GO nanosheets serve as nucleation centers for the in-situ growth of bimetallic CoPt nanoparticles. The reaction mixture is then removed from sonication and heated up to 590 K for 1 h in nitrogen ambient. Afterwards, the products are separated by centrifugation and washed by a 1/1 ethanol-hexane mixture in order to remove excess organic solvents and reaction by-products. Finally, the CoPt-decorated r-GO nanosheets are stored in toluene. Preliminary characterization, by means of X-ray diffraction and transmission electron microscopy, yields a maximum of 30 wt % coverage of r-GO with CoPt nanoparticles, and an average size from 5 nm to 7 nm for the latter. The presence of CoPt results in enhanced r-GO surface-functionalization with oleyl amine and slightly larger average nanosheet thickness. Oleyl amine-based functionalization yields stable suspensions

of spherical and anisotropic nanoparticles within LC matrices[26,27,33,34,45,48].

One mixture of CE8 and r-GO nanosheets has been prepared following precisely the protocol established and described in previous studies[26,27,49,50]. The r-GO concentration is defined as χ = 0.001, where $\chi = m_{r-GO}/(m_{CE8} + m_{r-GO})$, i.e. it is the mass of r-GO over the total sample mass. Immediately after their preparation the samples are loaded in home-made, high-purity silver cells for calorimetric measurements and in glass slides separated by 10 μm spacers for optical observations.

The heat capacity measurements have been performed by means of high-resolution ac calorimetry at Jožef Stefan Institute (Slovenia). The calorimetric aparatus is house-in-built and fully-automatized. A small heater and a glass-bead thermistor are attached on the silver cell containing the sample in order to supply the power to the sample and accurately measure its temperature. Additional thin copper wires thermally link the cell to the first copper shield that plays the role of bath. The heat capacity of the sample is obtained using the conventional ac mode of operation, which is mostly sensible to the continuous changes of enthalpy. In case of second order (continuous) transition this mode provides the exact temperature profile of heat capacity $C_p(T)$. First order (discontinuous) transitions are traced by an anomalous phase behavior along the phase coexistence region and an additional mode of operation can be used, the so-called relaxation or non-adiabatic scanning mode. The latter measures the total change of enthalpy, continuous and discontinuous, i.e. latent heat. The comparison of ac and relaxation mode data yields the latent heat of the transition. Additional details concerning the operation of ac calorimetry can be found elsewhere[51].

The optical measurements have been performed in University of Athens (Greece). The samples are placed and observed under a Leica DM2500P optical microscope in transmission mode. The temperature is slowly changed and stabilized at small intervals using an Instec HCS402 heating stage with temperature stability better than 10 mK. Images of the textures are captured under crossed polarizers using a Leica DFC420 digital camera in combination with LAS image acquisition software.

III. RESULTS AND DISCUSSION

The calorimetric results of the χ = 0.001 r-GO mixture, upon heating and cooling with a scanning rate of 0.25 Kh^{-1}, are presented on the upper two layers of Figure 1. The temperature profiles

of heat capacity $C_p(T)$ are plotted from well inside the I phase down to the N* phase. They show a reproducible blue phase range, being 7.6 K upon heating and 7.8 K upon cooling. The existence of only two anomalies between the I and the N* phases evinces the presence of one blue phase structure for the mixture. It is worth noting that the presented $C_p(T)$ profiles are obtained with the conventional ac mode, being sensitive mostly to the continuous part of enthalpy changes, hence they do not provide the total enthalpy change of first order phase transitions. This means that the heat capacity data are used to accurately determine the temperature range of BPs for bulk samples, but do not yield the total enthalpic content of the transitions.

The $C_p(T)$ profiles are essentially different compared to the pure CE8 where all three blue phases are present in a total temperature range of $\sim$ 5 K[26]. In particular, CE8 exhibits a 1.2 K range of BPIII, 0.8 K of BPII and 3.0 K of BPI, as confirmed by calorimetry and microscopy as shown in Figure 1. The $C_p(T)$ profiles of the χ = 0.001 mixture show only one blue phase present on both heating and cooling runs. Based on the outcome of previous results on anisotropic nanoparticles[33–35], this blue phase is expected to be BPI.

In order to obtain additional information on the (expected) BPI we have performed polarizing optical microscopy measurements. The microscopic observations have been performed upon slow heating and cooling cycles. The textures collected at selected temperatures upon cooling the mixture are presented in Figure 2. A foggy BPIII texture appears only along a few tens of mK range as a bluish front and immediately converts to large domains of apparently BPI. This metastable I-BPIII-BPI state apparently corresponds to the $\sim$ 180 mK wide first order region of the I-BPI transition seen in calorimetric data in Figure 1. It could be also additionally enhanced by the larger temperature oscillations in microscopy ($\sim$ 10 mK) with respect to ac calorimetry ($\sim$ 0.5 mK). In this region the isotropic domains acquire a BPIII structure that, under the influence of r-GO, gives rapidly its place to the large ordered domains of BPI. Afterwards, the BPI texture is stable for a temperature range over 7 K, in agreement with calorimetric results. Along this range only a gradual change of color occurs from blue to turquise upon cooling. This is related to progressive change of the pitch size with temperature. Upon further cooling the oily streaks texture characteristic of N* phase finally appear. The reproducibility of optical textures upon sequential heating and cooling combined with high-resolution calorimetric data provide robust evidence of a thermodynamically stable BPI structure. Note that the absolute temperatures exhibit a few mK difference between calorimetric and miscoscopic data. That is acceptable due to different thermometry and more stringent temperature control in case of calorimetry, as mentioned above.

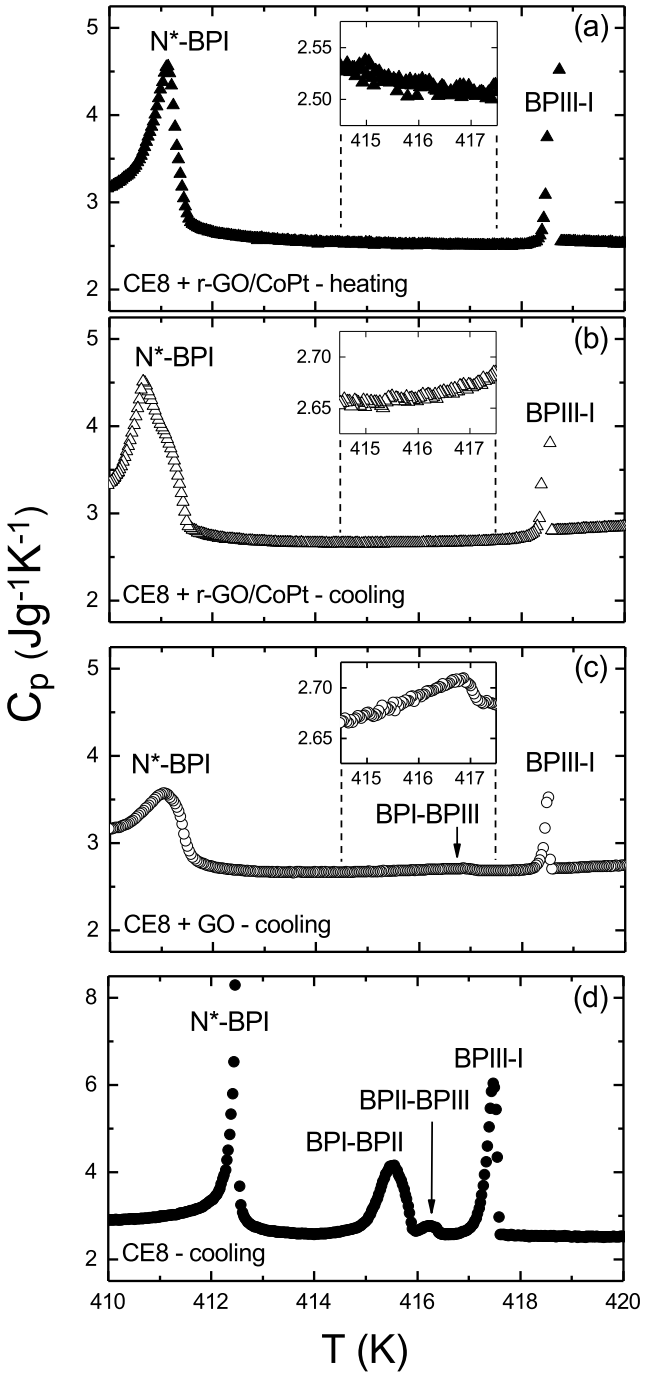

FIG. 1. The $C_p(T)$ profiles in the range from I down to N* phase are shown for (a) χ = 0.001 mixture of CE8 + r-GO/CoPt upon heating (solid triangles) and (b) χ = 0.001 mixture of CE8 +r-GO/CoPt upon cooling (open triangles) from present work. In addition, the corresponding profiles are shown for (c) χ = 0.001 mixture CE8 + GO upon cooling (open circles) from Ref.[34] and (d) of pure CE8 upon cooling (solid circles) from Ref.[26]. The inset on layer (c) provides a magnification of the small BPIII-BPI anomaly that is not clearly visible in the full-scale plot. Note that no anomaly is present in the insets of layers (a) and (b).

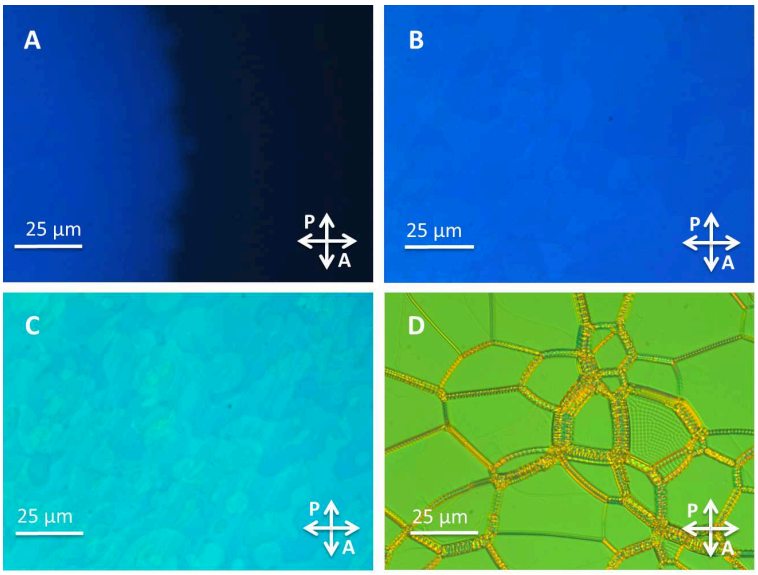

FIG. 2. Optical textures, obtained in transmission mode and under crossed polarizers, on cooling of $\chi = 0.001$ CE8 + r-GO mixture are presented here: (A) coexistence of isotropic (black), BPIII (foggy blue) and BPI (vivid blue) at 418.5 K, (B) BPI at 417 K, (C) BPI at 414.5 K and (D) N^* at 409 K.

Some similarities exist among the present results with CoPt-decorated r-GO and our previous work with non-decorated GO of same concentration $\chi = 0.001$[34]. As seen in Figure 1, the total blue phase range is similar, being 7.8 K for CoPt-decorated r-GO and 7.5 K for GO on cooling. In addition, there is a shift of the Isotropic to Blue Phase transition to higher values. This is identical in both cases, in the range of 1 K. This upshift of I-BPI or I-BPIII phase transition is in agreement with our previous work in CE8-dispersed nanosheets such as graphene oxide, molybdenum disulfide and laponite[33–35]. Moreover, several other studies in literature report an increase of the isotropic-to-blue-phase[36,37,52] or isotropic-to-nematic[53] phase transition temperature in the presence of graphene or graphene oxide nanosheets. It can be attributed to the wetting of large nanosheets that induce some order within the I phase upon cooling the samples[54].

A striking difference appears also between the two types of CoPt-decorated r-GO nanosheets and previous non-decorated GO dispersed in CE8. Only one phase, as proven by calorimetry and microscopy, namely the most ordered BPI is stabilized for CoPt-decorated r-GO. On the contrary, a BPIII and BPI sequence was observed for non-decorated graphene, with BPI being wider[34]. In the present study, as explained above, the BPIII is metastable along the $\sim$ 180 mK wide I-BPI phase coexistence range and essentially only BPI is thermodynamically stable. It is anticipated that the CoPt-enhanced coverage of r-GO surface with oleylamine promotes the essentially direct forma-

tion and stabilization of the most ordered blue phase structure, i.e. BPI.Note that the nanosheets' concentration used in the present r-GO, as well as in previous GO study[34], refers to a mass ratio. The concentration being the same (χ = 0.001) and the r-GO heavier (due to the presence of CoPt), the same effect on the total BP range and a larger effect on BPI are achieved here by an overall smaller number of nanosheets. This is a qualitative proof that the decorated r-GO nanosheets are more efficiently trapped within the disclination lines in comparison to their GO counterparts.

In the following we describe the key mechanisms that are responsible for the enhanced temperature stability range of BPI. The dominant liquid crystal-nanosheet free energy density contribution reads $f = -w\vec{e}.\boldsymbol{Q}\vec{e}$. Here the unit vector $\vec{e}$ stands for the interaction locally preferred orientational order, w is the representative anchoring strength constant, and $\boldsymbol{Q}$ is the nematic tensor order parameter, quantifying the degree of orientational order at the mesoscopic level. In the case of uniaxial order it is commonly expressed as $\boldsymbol{Q} = s(\vec{n} \otimes \vec{n} - \boldsymbol{I}/3)$, where s is the nematic order parameter measuring the amplitude of the orientational order, $\vec{n}$ is the nematic director field describing the local uniaxial orientation, and the states $\pm\vec{n}$ are physically equivalent. In case of strong elastic distortions, which are generated by disclinations, $\boldsymbol{Q}$ exhibits biaxial order[55]. In this case, the order parameter is expressed as $\boldsymbol{Q} = \sum_{i=1}^{3} \lambda_i \vec{e}_i \otimes \vec{e}_i$, where λ_i and $\vec{e}_i$ are the tensor's eigenvalues and eigenvectors, respectively.

For $w > 0$ the phase transition temperature between the isotropic and the orientationally ordered phases increases on increasing χ[34]. Furthermore, it is assumed that the easy direction is "adaptable", i.e. it could orient along the locally liquid crystal-imposed orientational order. In this case the defect core replacement (DCR) mechanism[16,26] could explain the increased temperature window of BPI stability with respect to the competing phases (BPII, BPIII). DCR assumes that the nanosheets assemble in regions possessing disclinations. Concequently, they partially replace the energetically costly disclinations' core volume with a trapped nanosheet's volume part. Note that the DCR mechanism is effective if nanosheets do not significantly distort the disclination-imposed nematic order. This condition is fulfilled by assuming an adaptive character of $\vec{e}$. In order to explain the enhanced stability of BPI structure with respect to the competing BPII and BPIII, we assume that the spatial arrangment of nanosheets is more compatible with the BPI disclination lattice structure[34].

In the case of spherical small NPs, such as CdSe quantum dots[26,27], it is rather straightfoward to expect that the latter aggregate in the cores of defects. Nevertheless, in the case of essentially larger but thin nanosheets that promote homeotropic anchoring of LC molecules, the arrangment

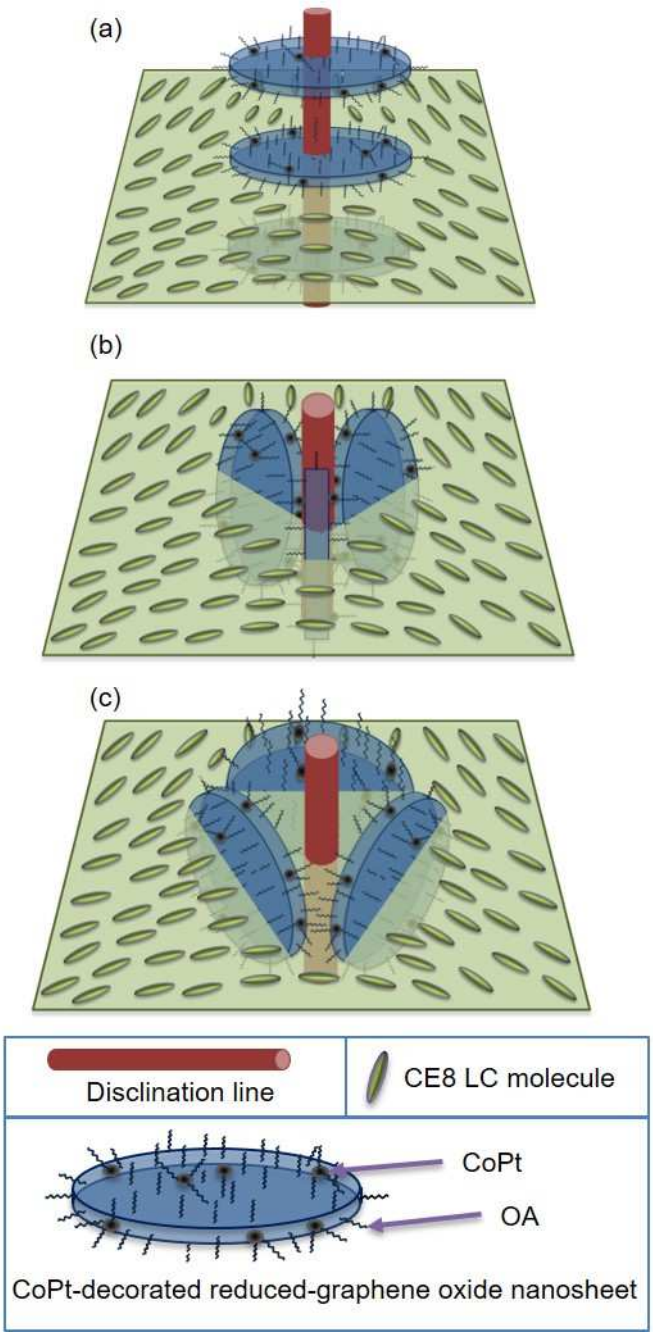

FIG. 3. A rough schematic representation of the possible configurations of CoPt-decorated r-GO nanosheets along the disclination lines is presented. All sizes are approximate and the LC molecules are shown only along one plane for clarity. The top scheme (a) represents a stack of nanosheets along the disclination line, whereas the middle and bottom schemes (b) and (c) a triangular configuration around it.

is not so obvious. One could assume that nanosheets are stacked along the disclination lines or arranged in triangular configurations. These possible configurations are schematically depicted in Figure 3. In the first case (of stacked nanosheets, Figure 3a) the DCR mechanism[16,26] can explain the stabilization effect if anchoring is rather weak so that nanosheets sticking from the core do not essentially perturb the LC ordering around disclination lines. In the second case (triangular configuration, Figure 3b), nanosheets are lying in three radial plains oriented perpendicular to the locally tangential director field around the $m = -\frac{1}{2}$ disclination line. Also in this case for the part of nanosheets within the core the DCR mechanism applies. The part that sticks out here does not perturb the director field. In the last case (triangular configuration, Figure 3c), each nanosheet orients perpendicular to the three main directions around the $m = -\frac{1}{2}$ disclination line where the director is radial. If the homeotropic anchoring is not particularly strong, the deformation of the director field would be negligible. However, since DCR does not apply in this case to reduce the total free energy, the stability of this triangular nanosheet structure is questionable. In addition, the proximity of nanosheets usually drives them to form stacked discotic clusters. It is anticipated that the aggregation of nanosheets within the disclination lines of BPs comprises an interesting topic to be further addressed by simulation studies.

IV. CONCLUSIONS

We have demonstrated a strong stabilization effect of Blue Phase I in CoPt-decorated reduced-graphene oxide nanosheets dispersed in CE8. High-resolution calorimetry and polarizing optical microscopy results are in agreement with a stable Blue Phase I for 7.6 K on cooling and 7.8 K on heating. The improved surface coverage of r-GO nanosheets with oleylamine compared to our previous work promotes the direct formation of the more ordered BPI, appearing directly upon cooling from I phase. The presentation of experimental results was accompanied by a short theoretical discussion. The presented results support strongly the recent findings about the usefulness of graphene on stabilizing blue phases and underline the important role of surface chemistry.

V. ACKNOWLEDGMENTS

M.L. acknowledge the support of Project P1-0125 of the Slovenian Research Agency. G.C. acknowledges the support of Project CZ.02.2.69/0.0/0.0/16_027/0008465 for Mobility of Re-

searchers under the Operational Programme Research, Development and Education and of Project PE3-1535 implemented within the framework of the Action "Supporting Postdoctoral Researchers." G.N. and I.L. acknowledge the support of THALES Project of the Operational Strategic Plan "Education and Lifelong Learning", co-financed by the European Social Fund and the State of Greece. S.Ž. work was supported by the Slovenian Research Agency of Project P1-0099 and COST action EUTOPIA (CA17139).

REFERENCES

[1]H. F. Gleeson, R. J. Miller, L. Tian, V. G*ö*rtz and J. W. Goodby, Liq. Cryst. **42**, 1–12 (2015).

[2]F. Reinitzer, Monatsh. Chem. **9**, 421–441 (1888) [English translation of the original article: A. Weiss, Liq. Cryst. **5**, 7-18 (1989).

[3]G. W. Gray, J. Chem. Soc. 3733 (1956).

[4]D. Coates and G. W. Gray, Phys. Lett. A **45A**, 115–116 (1973).

[5]M. A. Marcus and J. W. Goodby, Mol. Cryst. Liq. Cryst. **72**, 297–305 (1982).

[6]P. J. Collings, Phys. Rev. A **30**, 1990–1993 (1984).

[7]K. Tanimoto, P. P. Crooker and G. C. Koch, Phys. Rev. A **32**, 1893-1895 (1985).

[8]D. K. Yang and P. P. Crooker, Phys. Rev. A **35**, 4419–4423 (1987).

[9]J. Thoen, Phys. Rev. A **37**, 1754–1759 (1988).

[10]G. Voets and W. Van Dael, Liq. Cryst. **14**, 617–627 (1993).

[11]E. P. Koistinen and P.H. Keyes, Phys. Rev. Lett. **74**, 4460–4463 (1995).

[12]Z. Kutnjak, C. W. Garland, C. G. Schatz, P. J. Collings, C. J. Booth and J. W. Goodby, Phys. Rev. E **53**, 4955–4963 (1996).

[13]M. A. Anisimov, V. A. Agayan and P. J. Collings, Phys. Rev. E **57**, 582–595 (1998).

[14]P. Etchegoin, Phys. Rev. E **62**, 1435–1437 (2000).

[15]W. Cao, A. Muñoz, P. Palffy-Muhoray and B. Taheri, Nat. Mater. **1**, 111-113 (2002).

[16]H. Kikuchi, M. Yokota, Y. Hisakado, H. Yang and T. Kajiyama, Nat. Mater. **1**, 64–68 (2002).

[17]S-Y. Jo, S-W. Jeon, B-C. Kim, J-H. Bae, F. Araoka and S-W. Choi, Appl. Mater. Interf. **9**, 8941–8947 (2017).

[18]J. Yan, Q. Li and K. Hu, J. Appl. Phys. **114**, 153104 (2013).

[19]O. Chojnowska, R. Dabrowski, J. Yan, Y. Chen and S.T. Wu, J. Appl. Phys. **116**, 213505 (2014).

[20]M. Nakata, Y. Takanishi, J. Watanabe and H. Takezoe, Phys. Rev. E **68**, 041710 (2003).

[21]I. Gvozdovskyy, Liq. Cryst. **42**, 1391–1404 (2015).

[22]H. J. Coles and M. N. Pivnenko, Nature **436**, 997–1000 (2005).

[23]A. Yoshizawa, Y. Kogawa, K. Kobayashi, Y. Takanishi and J. Yamamoto, J. Mater. Chem. **19**, 5759–5764 (2009).

[24]H. Choi, H. Higuchi, Y. Ogawa, H. Kikuchi, Appl. Phys. Lett. **101**, 131904 (2012).

[25]H. Yoshida, Y. Tanaka, K. Kawamoto, H. Kubo, T. Tsuda, A. Fujii, S. Kuwabata, H. Kikuchi and M. Ozaki, Appl. Phys. Express **2**, 121501 (2009).

[26]E. Karatairi, B. Rožič, Z. Kutnjak, V. Tzitzios, G. Nounesis, G. Cordoyiannis, J. Thoen, C. Glorieux and S. Kralj, Phys. Rev. E **81**, 041703 (2010).

[27]G. Cordoyiannis, P. Losada-Pérez, C.S.P. Tripathi, B. Rožič, U. Tkalec, V. Tzitzios, E. Karatairi, G. Nounesis, Z. Kutnjak, I. Muševič, C. Glorieux, S. Kralj and J. Thoen, Liq. Cryst. **37**, 1419–1426 (2010).

[28]I. Dierking, W. Blenkhorn, E. Credland, W. Drake, R. Kociuruba, B. Kayser and T. Michael, Soft Matter **8**, 4355–4362 (2012).

[29]L. Wang, W. He, Z. Xiao, F. Meng, Y. Zhang, P. Yang, L. Wang, J. Xiao, H. Yang and Y. Lu, Small **8**, 2189–2193 (2012).

[30]A. Sharma, M. Worden and T. Hegmann, Ferroelectrics **431**, 154–163 (2012).

[31]M. A. Gharbi, S. Manet, J. Lhermitte, S. Brown, J. Milette, V. Toader, M. Sutton and L. Reven, ACS Nano **10**, 3410–3415 (2016).

[32]F. Liu, G. Ma and D. Zhao, Nanotechnology **29**, 285703 (2018).

[33]M. Lavrič, G. Cordoyiannis, S. Kralj, V. Tzitzios, G. Nounesis and Z. Kutnjak, Appl. Opt. **52**, E47-E52 (2013).

[34]M. Lavrič, V. Tzitzios, S. Kralj, G. Cordoyiannis, I. Lelidis, G. Nounesis, V. Georgakilas, H. Amenitsch, A. Zidanšek and Z. Kutnjak, Appl. Phys. Lett. **103**, 143116 (2013).

[35]M. Lavrič, V. Tzitzios, G. Cordoyiannis, S. Kralj, G. Nounesis, I. Lelidis and Z. Kutnjak, Mol. Cryst. Liq. Cryst. **615**, 14-18 (2015).

[36]Y. Zhao, X. Qiao, K. Li, S. Ding, S. Tian, H. Ren, M. Zhu, Q. Ma, Y. Zhao, W. Ban and Z. Miao, Mol. Cryst. Liq. Cryst. **664**, 1–8 (2018).

[37]W. Zhang, X. Wang, D. Wang, Z. Yang, H. Gao, Y. Zing, W. He, H. Cao and H. Yang, Liq. Cryst. **43**, 573–580 (2016).

[38]B. Rožič, V. Tzitzios, E. Karatairi, U. Tkalec, G. Nounesis, Z. Kutnjak, G. Cordoyiannis, R. Rosso, E. G. Virga, I. Muševič and S. Kralj, Eur. Phys. J. E **34**, 17 (2011).

[39]O. Henrich, K. Stratford, M.E. Cates and D. Marenduzzo, Phys. Rev. Lett. **106**, 107801 (2011).

[40]J. Fukuda, Phys. Rev. E **86**, 041704 (2012).

[41]S. M. Shamid, D. W. Allender and J. V. Selinger, Phys. Rev. Lett. **113**, 237801 (2014).

[42]A. C. Pawsey and P. S. Clegg, Soft Matter **11**, 3304-3312 (2015).

[43]J. A. Martínez-González, Y. Zhou, M. Rahimi, E. Bukusoglu, N. L. Abbott and J. J. de Pablo, Proc. Natl. Acad. Sci. **112**, 13195-13200 (2015).

[44]S. Ni., H. Li, S. Li., J. Zhu, J. Tan, X. Sun, C.P. Chen, G. He, D. Wu, K.-C. Lee, C.-C. Lo, A. Lien, J. Lu and Y. Su, J. Mater. Chem. C **2**, 1730–1735 (2014).

[45]M. Lavrič, G. Cordoyiannis, V. Tzitzios, S. Kralj, G. Nounesis, I. Lelidis, H. Amenitsch and Z. Kutnjak, Liq. Cryst. DOI: 10.1080/02678292.2019.1680757.

[46]D.V. Stergiou, E.K. Diamanti, D. Gournis and M.I. Prodromidis, Electrochem. Commun. **12**, 1307–1309 (2010).

[47]V. Tzitzios, K. Dimos, S.M. Alhassan, R. Mishra, A. Kouloumpis, D. Gournis, N. Boukos, M.A. Roldan, J.-C. Idrobo, M.A. Karakassides, G. Basina, Y. Alwahedi, H.J. Kim, M.S. Kasiotis, M. Fardis, A. Borisevich, S.J. Pennycook, S.T. Pantelides and G. Papavassiliou, Front. Mater. **5**, 29 (2018).

[48]G. Cordoyiannis, V. S. R. Jampani, S. Dhara, S. Kralj, V. Tzitzios, G. Basina, G. Nounesis, Z. Kutnjak, C. S. P. Tripathi, P. Losada-Pérez, D. Jesenek, C. Glorieux, I. Muševič, A. Zidanšek, H. Amenitsch and J. Thoen, Soft Matter **9**, 3956–3964 (2013).

[49]H. Haga and C. W. Garland, Phys. Rev. E **56**, 3044-3052 (1997).

[50]G. Cordoyiannis, S. Kralj, G. Nounesis, Z. Kutnjak and S. Žumer, Phys. Rev. E **75**, 021702 (2007).

[51]H. Yao, K. Ema and C. W. Garland, Rev. Sci. Instrum. **69**, 172-178 (1998).

[52]S. Al-Zangana, M. Iliut, M. Turner, A. Vijayaraghavan and I. Dierking, Adv. Opt. Mater. **4**, 1541-1548 (2016).

[53]S. Javadian, N. Dalir and J. Kakemam, Liq. Cryst. **44**, 1341-1355 (2017).

[54]I. Lelidis and P. Galatola, Phys. Rev. E **66**, 010701 (2002).

[55]N. Schopohl and T. J. Sluckin, Phys. Rev. Lett. **59**, 2582-2584 (1987).